JOURNAL OF GEOPHYSICAL RESEARCH, VOL. 100, NO. A3, PAGES 3427–3437, MARCH 1, 1995

Wave and ion evolution downstream of quasi-perpendicular bow shocks

M. E. McKean, N. Omidi,[1] and D. Krauss-Varban
Department of Electrical and Computer Engineering, University of California, San Diego, La Jolla

Abstract. Distribution functions of ions heated in quasi-perpendicular bow shocks have a large perpendicular temperature anisotropy that provides free energy for the growth of Alfvén ion cyclotron (AIC) waves and mirror waves. Both types of waves have been observed in the Earth's magnetosheath downstream of quasi-perpendicular shocks. The question of whether these waves are produced at the shock and convected downstream or whether they are produced locally in the magnetosheath has not yet been answered. If the latter were true, then under most magnetosheath conditions AIC waves should dominate the wave activity, yet frequently mirror waves either dominate or are competitive with the AIC mode. We address this question by using two-dimensional hybrid simulations to give a self-consistent description of the evolution of the wave spectra downstream of quasi-perpendicular shocks. Both mirror and AIC waves are identified in the simulated magnetosheath. They are generated at or near the shock front and convected away from it by the sheath plasma. Near the shock, the waves have a broad spectrum, but downstream of the shock, shorter-wavelength modes are heavily damped and only longer-wavelength modes persist. The characteristics of these surviving modes can be predicted with reasonable accuracy by linear kinetic theory appropriate for downstream conditions. Throughout the downstream region, the power in compressive magnetic oscillations is of the same order as the power in transverse oscillations. We also follow the evolution of the ion distribution function. The shocked ions that provide the free energy for wave growth have a two-component distribution function: a core population of directly transmitted ions and a smaller halo of initially reflected ions that contains the bulk of the free energy. The halo is initially gyrophase-bunched and extremely anisotropic. Within a relatively short distance downstream of the shock (of the order of 10 ion inertial lengths), wave-particle interactions remove these features from the halo and reduce the anisotropy of the distribution to near-threshhold levels for the mirror and AIC instabilities. A similar evolution has been observed for ions at the Earth's bow shock.

1. Introduction

Ions incident on quasi-perpendicular shocks are known to be preferentially accelerated and energized within the shock front in the directions perpendicular to the average magnetic field. Consequently, the ion population in the immediate vicinity of the shock front has a large temperature anisotropy ($T_\perp > T_\parallel$), which can provide free energy for the growth of ion waves. In particular, two instabilities are known to be driven by anisotropic ion distributions: (1) the mirror instability, an oblique, compressive mode with magnetic fluctuations primarily parallel to the average magnetic field $\vec{B}_o$ [*Chandrasekhar et al.*, 1958; *Barnes*, 1966; *Hasegawa*, 1975]; and (2) the Alfvén ion cyclotron (AIC) instability, a mode with maximum growth along $\vec{B}_o$ and magnetic fluctuations primarily perpendicular to the average field [*Kennel and Petschek*, 1966; *Davidson and Ogden*, 1975].

Evidence for both of these instabilities have been found in the quasi-perpendicular magnetosheath of the Earth [*Lacombe et al.*, 1989, 1992; *Anderson et al.*, 1991; *Fuselier et al.*, 1991; *Anderson and Fuselier*, 1993]. In gyrotropic, homogeneous electron-proton plasmas, linear kinetic theory has shown that, for $\beta_{i\parallel} < 6.0$ (where $\beta_{i\parallel}$ is the proton beta associated with $T_\parallel$), the AIC instability has a larger growth rate and a lower anisotropy threshhold than the mirror instability [*Gary*

[1] Also at California Space Institute, University of California, San Diego, La Jolla.

Paper number 94JA02529.
0148-0227/95/94JA-02529$05.00

et al., 1976; *Gary*, 1992]. This conclusion has received support from quasi-linear theory [*Yoon*, 1992]. From these results, one would expect little or no mirror wave activity to be found in the magnetosheath. However, spacecraft not only detect mirror waves, their observations show that these waves often dominate the wave activity and sometimes reach large amplitudes ($\delta B/B_o \sim 1$) [*Tsurutani et al.*, 1982; *Moustaizis et al.*, 1986; *Hubert et al.*, 1989; *Anderson and Fuselier*, 1993].

Two explanations have been given for this inconsistency between observations and theoretical expectations. *Price et al.* [1986] showed that the presence of He^{++} can suppress the AIC instability while leaving the mirror instability unaffected, thus enhancing the mirror mode relative to the Alfvén mode. This conclusion was supported by the theoretical results of *Gary et al.* [1993]. Specifically, they found that in the presence of helium ions, the mirror mode should dominate the AIC mode for high-beta ($\beta \gtrsim 1$), low-anisotropy conditions ($T_\perp/T_\parallel \lesssim 2$), while the AIC mode should dominate under low-beta, high-anisotropy conditions. This theoretical result received support from observations near the magnetopause by *Anderson and Fuselier*[1993] and the results of numerical particle simulations [*Gary et al.*, 1993, 1994].

The second explanation, advanced by *Omidi et al.* [1994], is that the mirror and AIC wave activity observed in the magnetosheath is generated at or near the shock front and then convected further downstream. Because of the impulsive heating of incident ions at the shock, the temperature anisotropy is at its greatest by the shock, and hence both the mirror and AIC waves should grow very rapidly. The plasma inhomogeneities near the shock suggest that homogeneous treatments are inadequate to model this wave growth. Also, with a few exceptions [e.g., *Brinca et al.*, 1990], past homogeneous treatments have not properly modeled the finer details of the shocked ion distribution function. Finally, most homogeneous treatments do not take into account the driven nature of the shock-magnetosheath system. The combination of these factors could make the mirror instability competitive with or even dominant over the AIC instability. As the waves are convected downstream, the temperature anisotropy is maintained at a level close to the threshhold for either one or both of the instabilities. This means that one and possibly both modes are only weakly damped, which allows the waves to be convected far downstream with only small changes in amplitude. Note that this explanation does not take into account certain macroscale phenomena, such as the compression of magnetic field lines in the magnetosheath [*Zwan and Wolf*, 1976], that could change the anisotropy and beta of the plasma near the magnetopause.

The second explanation appears to be supported by observations by *Sckopke et al.* [1983, 1990] that show intense wave activity at the shock front, followed by a reduction in wave energy as one moves away from the shock. Whether compressional or transverse fluctuations dominate the downstream activity is dependent upon upstream parameters such as the beta and the Mach number of the shock [*Sckopke et al.*, 1990]. However, the wave modes in these observations have not been clearly identified nor has the evolution of the spectra been followed in detail.

In this paper, we investigate this second explanation by using two-dimensional hybrid simulations to model quasi-perpendicular shocks and the self-consistent evolution of the plasma downstream. We use recently developed diagnostic methods to identify the wave modes that exist downstream of the shock and to follow the evolution of the wave spectra [*Omidi et al.*, 1994]. In addition, we measure the feedback of the waves on the ions by following the evolution of the ion distributions and contrasting the particle data with the wave data. This analysis concentrates on the evolution of electron-proton plasmas so that the effect of heavier ion species on the competition between the mirror and AIC instabilities can be considered separately.

The first simulation study that showed that mirror waves can indeed be excited downstream of quasi-perpendicular shocks was carried out by *Lee et al.* [1988]. This study used one-dimensional simulations which are limited by the fact that waves can only propagate at a single angle with respect to the magnetic field and hence the mirror and AIC instabilities are prevented from competing effectively [*Lee et al.*, 1988]. Using a two-dimensional hybrid simulation, *Winske and Quest* [1988] were able to demonstrate that both compressional and transverse waves were excited downstream of a quasi-perpendicular shock. They concluded that the AIC mode dominates the wave activity based primarily on the measurement of the parallel wavenumber. This conclusion was only tentative, however, because the authors were unable to accurately identify other linear properties of the waves, such as frequency and perpendicular wavenumber, and hence could not pinpoint individual modes. To rectify their difficulties, we have developed diagnostic methods that enable us to identify the frequencies and both components of the wavenumbers of the downstream waves and thus identify these waves with linear modes.

In section 2 of this paper, we describe the model used to simulate the shock and magnetosheath and examine the magnetic and temperature profiles of the simulated system. In section 3, we describe the nature of the downstream wave activity and how the wave spectra evolve with increasing distance from the shock. Included in this section is a discussion of the changing linear properties of the waves. In section 4, we examine how the ion distribution changes with distance from the shock and relate it to the wave data. A summary and conclusions are presented in section 5.

2. Shock Structure

The two-dimensional hybrid code is similar to that used by *Omidi et al.* [1994], and uses a predictor-corrector method to solve for the electromagnetic fields [*Byers et al.*, 1978]. The simulation system is set in the

$x-y$ plane, which is also the plane of the background magnetic field. It has the dimensions $L_x = 200c/\omega_p$ and $L_y = 100c/\omega_p$, where L_x and L_y are the lengths in the x and y directions, respectively, c is the speed of light, and ω_p is the upstream ion plasma frequency. The system is superimposed on a grid that has cells of dimensions $\Delta x = \Delta y = 0.5c/\omega_p$. Particle positions, velocities and electromagnetic fields are updated once every time step $\Delta t = 0.007\Omega_p^{-1}$, where Ω_p is the ion gyrofrequency in the upstream region. The ratio v_A/c is 10^{-4}, where v_A is the Alfvén speed. Ions incident on the right boundary ($x = 200c/\omega_p$) are reflected, while those that cross the left boundary are lost to the system. Periodic boundary conditions are used in the y direction.

At the start of the run the simulation plasma consists of a flux of ions moving in the positive x direction and a co-moving, neutralizing, massless electron fluid. This ion flux models the upstream plasma incident on the quasi-perpendicular shock, and is maintained throughout the simulation by continuous injection of ions from the left-hand boundary. A stationary downstream plasma forms as the result of the interaction between the incoming flux and the ions reflected off the right boundary, and a fast shock forms at the boundary between this plasma and the upstream ions. The Alfvén Mach number M_A of the shock, the angle θ_{Bn} between the upstream magnetic field $\vec{B}_o$ and the shock normal (which points in the $-x$ direction), the ion beta β_i, and the electron β_e are all input parameters. The velocity v_i of the incident beam and the right-side (downstream) magnetic field $\vec{B}_1$ at the right-hand boundary are determined from these inputs by the Rankine-Hugoniot conditions. The simulation frame is equivalent to the downstream rest frame, so in the simulation frame, the shock moves steadily to the left.

For this study, we chose to examine quasi-perpendicular shocks with Mach numbers significantly higher than the critical Mach number M_c, defined in MHD shock theory as the limit beyond which resistivity alone cannot provide all the necessary dissipation at the shock. Most of the time, the Earth's bow shock forward of the terminator line belongs to this supercritical class. For such supercitical bow shocks, the plasma beta is usually relatively high, i.e., of order unity. Thus for our simulations we chose $M_A = 8$, $\theta_{Bn} = 80°$, and $\beta_i = \beta_e = 0.5$. For these parameters, the incident normal velocity (in the downstream = simulation frame) $v_i = 5.8v_A$ and downstream magnetic field $B_1 = 3.57B_o$.

This simple model of the quasi-perpendicular bow shock and magnetosheath does not account for such macroscale phenomena as the compression of magnetic field lines which occurs as the sheath plasma approaches the magnetopause. This compression probably is responsible for the change in plasma characteristics observed in the region close to the magnetopause [*Anderson and Fuselier*, 1993]. Wave properties are also observed to change in this region. However, throughout most of the magnetosheath the compression of the magnetic field is not strong enough to change the plasma properties significantly, and the wave spectrum changes only slightly. Thus the conclusions drawn from these simulation results should be applicable to the bulk of the quasi-perpendicular magnetosheath, not just in the vicinity of the shock.

The profile of magnetic field component B_y at $\Omega_i t = 61$ as a function of x and y is shown in Figure 1a. Profiles of B_y as a function of x for three different values of y are shown in Figure 1b. Because $\vec{B}_o$ (the magnetic field averaged over y) is approximately parallel to the y axis ($\theta_{Bn} = 80°$ upstream and 87° downstream), the profile shown here is essentially the sum of B_o and fluctuations parallel to it. The magnetic structure of this simulated shock is essentially the same as that of observed shocks. Within the shock ramp, B_y increases rapidly, reaching a maximum (as high as $7B_o$) in the

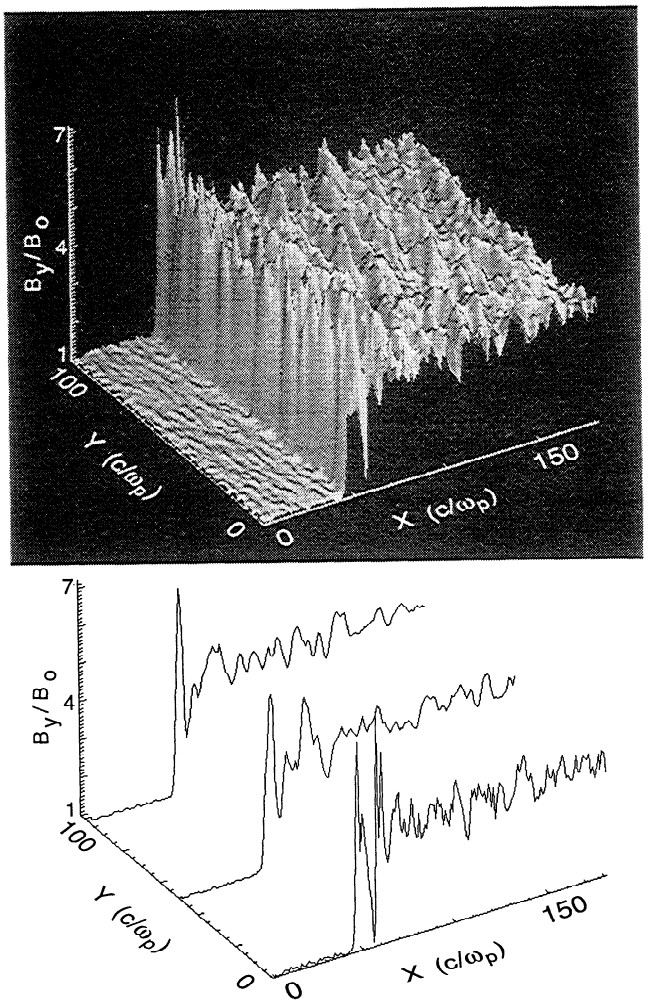

Figure 1. Profiles of B_y (in units of upstream field B_o) at $\Omega_p t = 61$ (top) in a three-dimesnional representation as a function of x and y; and (bottom) as a function of x for three different values of y. Values x and y are plotted in terms of the upstream ion inertial length c/ω_p. The shock front is located at approximately $x = 48c/\omega_p$. Fluctuation amplitudes are largest immediately behind the shock, and decrease monotonically thereafter. Downstream wave amplitudes are about 10% of the ambient field strength.

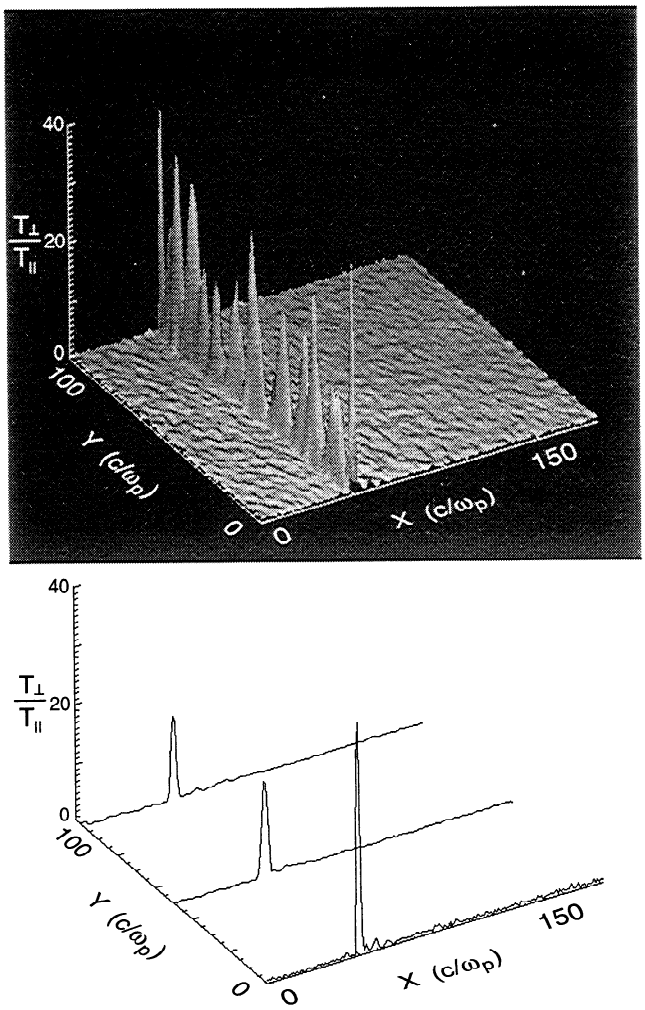

Figure 2. Profiles of the ion temperature anisotropy $T_\perp/T_\parallel$ at $\Omega_p t = 61$ (top) in a three-dimensional representation as a function of x and y; and (bottom) as a function of x at three different values of y. The anisotropy rises rapidly in the shock front, reaching a maximum of about 40 at about the magnetic overshoot, and then declines almost as fast to threshhold levels for the excitation of ion instabilities.

shock overshoot at about $x \simeq 50c/\omega_p$. Then B_y decreases rapidly in the undershoot region ($x \simeq 57c/\omega_p$). The magnitudes of fluctuation amplitudes decrease as one moves away from the shock, but fluctuations with amplitude $\delta B_y \sim 0.1B_1$ persist to the right side of the simulation system. The phase fronts of the waves are almost parallel to the y axis or shock normal, i.e., the waves appear to be propagating at large angles with respect to the average downstream magnetic field, consistent with mirror waves.

Figure 2 shows the profile of the temperature aniso tropy $T_\perp/T_\parallel$ at the same time, and in the same manner, as Figure 1. The anisotropy rises rapidly within the shock ramp and reaches a peak value at about the magnetic overshoot. This peak value varies as a function of y from a few to about 40. The variation is due to the fact that the fraction of incident ions specularly reflected at the shock is a nonuniform function of y and the specularly-reflected ions are responsible for most of the anisotropy seen at the shock. After reaching its peak, the anisotropy declines rapidly to values below 2.0 over a distance of only about $10c/\omega_p$, presumably as a result of the large-amplitude wave activity in this region (cf. Figure 1). The anisotropy declines more slowly as the plasma moves further away from the shock until at $x = 180c/\omega_p$, $T_\perp/T_\parallel \simeq 1.2$. This is roughly the threshhold value for excitation of the AIC instability for $\beta_i = 5.5$ (the approximate downstream value). In contrast, the mirror mode is weakly damped at low k.

Figure 3 shows profiles of the magnetic field magnitude B, the ion density n, the ion temperatures perpendicular ($T_\perp$) and parallel ($T_\parallel$) to the magnetic field, and the logarithm of ($T_\perp/T_\parallel$-1) as functions of x. All quantities are calculated for each individual cell and are then averaged over y. The magnetic field magnitude reaches an average value of about $4B_o$ in the overshoot before falling to its downstream value of about 3.3 B_o, while the density reaches an average value of about $4.75n_o$ before falling to a downstream value of about $3.2n_o$. The perpendicular temperature also reaches a peak (about $50T_o$) in the overshoot, but $T_\parallel$ climbs more slowly. In the overshoot $T_\parallel \simeq 4T_o$ and hence the average anisotropy $T_\perp/T_\parallel \simeq 12.5$. The anisotropy drops

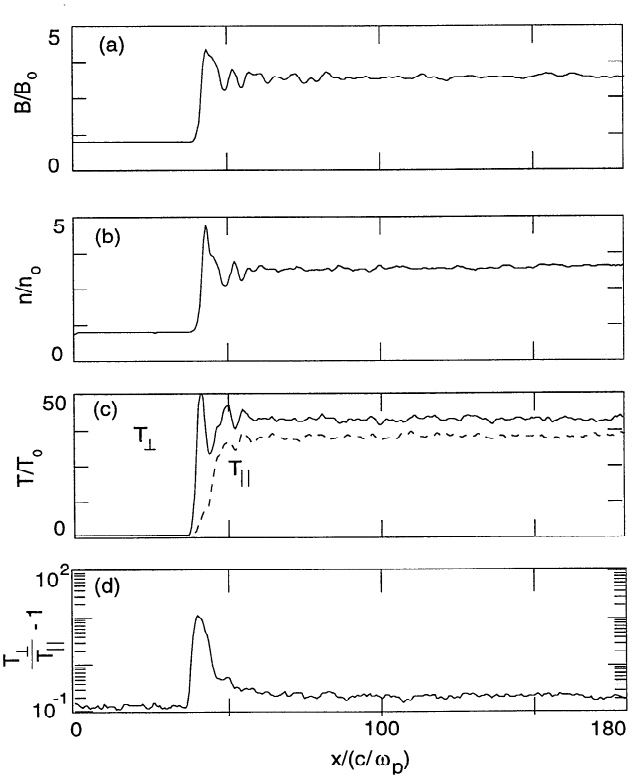

Figure 3. Profiles of certain plasma parameters at $\Omega_p t = 61$. Shown as functions of x (averaged over y) are (a) the magnetic field magnitude B (in units of B_o, the upstream field); (b) the ion density n (in units of the upstream density n_o); (c) the perpendicular temperature $T_\perp$ (solid line) and parallel temperature $T_\parallel$ (dashed line) of the ions (in units of the upstream ion temperature T_o); and (d) the ion temperature anisotropy $T_\perp/T_\parallel$.

rapidly, however, as wave-particle interactions heat the ions in the parallel direction until $T_{\|}$ reaches its approximate downstream value of $35T_o$. In this region, $T_\perp \simeq 42T_o$, making the average downstream anisotropy about 1.2.

3. Evolution of Waves

In this section, we analyze the evolution of the wave activity downstream of the shock. The top panel in Figure 4 shows the profiles of power as a function of compressional field oscillations (solid line), transverse oscillations in the $x-y$ plane (dashed line), and transverse oscillations out of the plane (heavy dashed line).

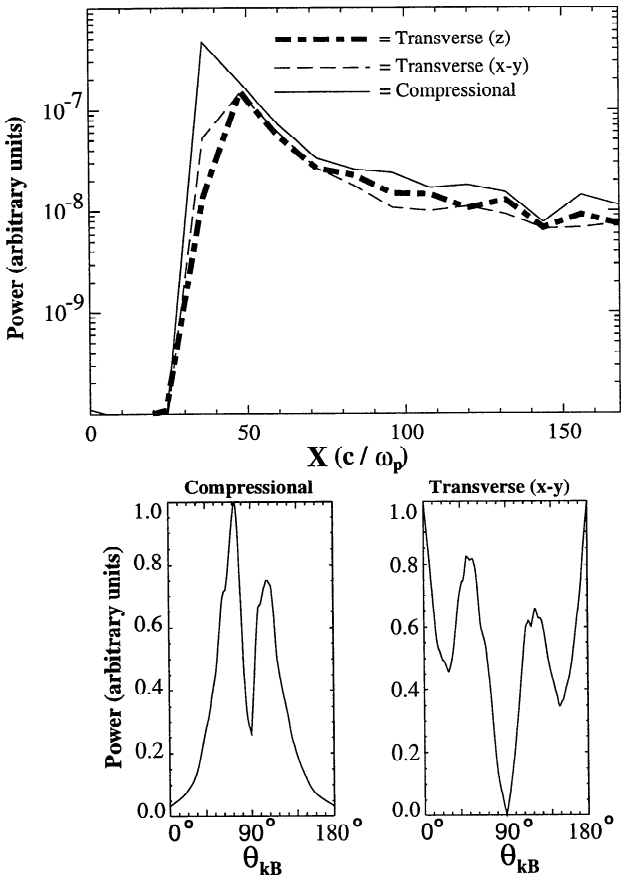

Figure 4. (Top) Profiles of the power in compressional fluctuations (solid line), coplanar ($x-y$ plane) transverse fluctuations (dashed line), and noncoplanar (z direction) fluctuations (thick dashed line), all shown as functions of x with an average taken over all y. In addition, each point represents an average over 8 c/ω_p. The fluctuation power is determined after the average field for a particular point has been subtracted out. The peak in compressional oscillations is caused by the shock front. The power in all three components is of the same order for $x \gtrsim 50c/\omega_p$. (Bottom, left) Compressional power as a function of propagation angle θ_{kB}. The dominant modes propagate at $\theta_{kB} = 71°, 59°$ and 109° in order of declining power. (Bottom, right) Coplanar transverse power of a function of θ_{kB}. The dominant modes propagate parallel and antiparallel to the average magnetic field.

The power in both compressional and transverse components rises about 3 orders of magnitude at the shock front, with the higher peak in the compressional component caused by the shock itself. Following this peak, the power in all three components decays steadily with x, although this decay slows considerably for $x > 70c/\omega_p$. Throughout the region to the right of the transverse peaks, the power in compressional oscillations is slightly greater than that in either transverse component, although the total power in transverse oscillations is equal to or greater than the compressional power at some locations.

The plots in the bottom panels of Figure 4 are based upon Fourier transforms of the magnetic fluctuation data at $\Omega_p t = 60.2$ in the region between $x = 112c/\omega_p$ and $181c/\omega_p$. This region is far enough from the shock front to be relatively free of the inhomogeneities associated with the shock and hence corresponds to the approximately homogeneous portion of the Earth's magnetosheath. The panels plot power (normalized to the peak in each case) against propagation angle θ_{kB} of compressional modes (left) and coplanar ($x-y$ plane) transverse modes (right). Compressional modes mostly propagate at highly oblique angles to the magnetic field, with the peak power located at $\theta_{kB} = 71°$ and secondary maxima at $\theta_{kB} = 59°$ and 109°. An analysis of the compressional spectrum as a function of x shows that the peak power is located at 59° near the shock front. The power at this angle decreases as one moves downstream until the peak at 71° becomes the dominant one. This behavior is consistent with the mirror mode because the propagation angle corresponding to maximum growth increases with decreasing anisotropy. Coplanar transverse modes mostly propagate parallel and antiparallel to the magnetic field lines, consistent with the AIC mode. Secondary peaks in the right panel are located at approximately the same angles as the peaks in the left panel. This is consistent with mirror waves, which have magnetic fluctuations in the coplanar transverse direction that are smaller than those in the parallel direction.

Figure 5 displays the power spectra for the angles of propagation corresponding to peak intensity for compressional oscillations (Figure 5a) and primary and secondary peak intensities for noncoplanar transverse oscillations (Figures 5b and 5c, respectively). Note that, in Figure 5 only, ω and kc are scaled in terms of the downstream cyclotron and plasma frequencies, respectively. These spectra are calculated for the simulation frame, which has the same x velocity as the downstream rest frame but has a small, nonzero v–y. In each case, the integration for the Fourier transforms was performed between $x/(c/\omega_p) = 112$ and 181 and between $\Omega_p t = 31.5$ and 63, i.e., the second half of the run. The shock front is located at $x \simeq 121c/\omega_p$ at the start of this time and at $x \simeq 42c/\omega_p$ at the end. Plotted over the spectra are ω–k dispersion curves in the simulation frame for the mirror mode at $\theta_{kB} = 59°$ (Figure 5a) and the AIC mode at $\theta_{kB} = 0^o$ (Figure 5b) and $\theta_{kB} = 59°$ (Figure 5c). The dispersions are calculated using linear theory of a ho-

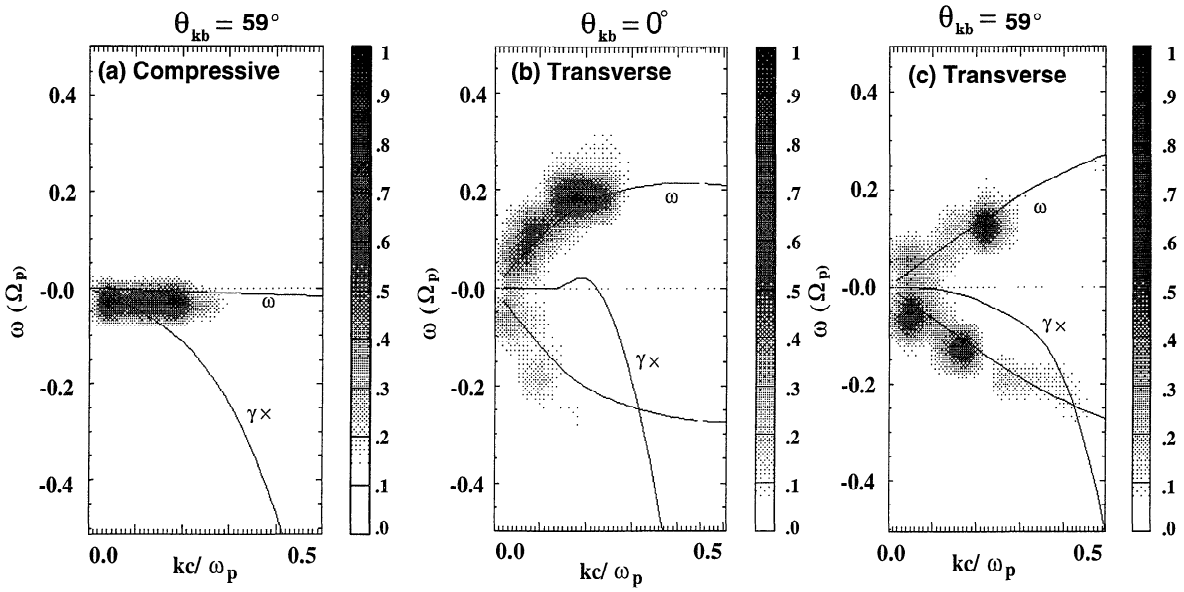

Figure 5. Power spectra for (a) compressional modes propagating at $\theta_{kB} = 59°$ and noncoplanar transverse modes propagating at (b) $\theta_{kB} = 0°$ and (c) $\theta_{kB} = 59°$. Plotted over the spectra is (a) the dispersion of the mirror mode and (b and c) the dispersion curves of the Alfvén ion cyclotron mode, including both the parallel and antiparallel modes. Both the real frequency (ω) and the growth rate (γ) are plotted, the latter at $10\times$ its actual value. The values for Ω_p and ω_p are those corresponding to the downstream magnetic field and density. The methods used for calculating both the spectra and the dispersions is described in the text.

mogeneous, bi-Maxwellian plasma with $T_\perp/T_\parallel = 1.25$ and $\beta_i = 5.5$. Both the forward and backward propagating Alfvén modes are shown in Figures 5b and 5c. For both the compressional and transverse fluctuations, the modes that dominate the power spectra fall on or close to the dispersion curves, demonstrating that the compressional fluctuations are associated with mirror waves and the transverse fluctuations with AIC waves. Consistent with this picture is the fact that the dominant modes correspond to $\omega - k$ values that are either undamped or only slightly damped according to linear theory.

Parallel-propagating AIC waves are strong in both δB_z and δB_x, indicating that these waves are approximately circularly polarized as expected. Helicity measurements indicate that these waves are predominantly left-hand circularly polarized. Obliquely propagating cyclotron waves are approximately linearly polarized, as expected from linear theory. The most intense of these modes propagates at about the same angles as the more intense mirror modes (for example, at $\theta_{kB} = 59°$). The ratio of power in oblique AIC waves to power in parallel AIC waves is greatest at the shock itself. This suggests that the nonlinearity of the shock system and transient features in the proton distribution (such as the gyrophase bunching of reflected protons) are important to the generation of the oblique waves. As the shocked plasma moves away from the shock, the ratio of oblique AIC wave power to parallel AIC wave power decreases. For polarization this implies that far from the shock the AIC wave activity is dominated by left-handed modes while near the shock, linearly polarized modes play a stronger role. This result is in qualitative agreement with the polarization measurements of transverse oscillations at low Mach number shocks [*Sckopke et al.*, 1990]. Measurements made downstream of one high Mach number shock by *Sckopke et al.* [1990] are more inconclusive; they indicate that transverse oscillations have no clear polarization most of the time. However, this is not necessarily inconsistent with our result. Polarization measurements by spacecraft would include contributions from transverse oscillations associated with mirror waves, which are strong downstream of high Mach number shocks though not low Mach number shocks. As a result of the Doppler shift, the mirror waves observed by spacecraft often have frequencies comparable to those of AIC waves and hence their transverse oscillations may be difficult to distinguish from AIC waves, complicating polarization measurements. In our analysis of simulation results, we can exclude the zero-frequency mirror mode oscillations from the helicity measurement and hence identify the dominant polarization of AIC waves. But if we do include the mirror mode, this identification becomes much harder.

Note that the linear growth rates for the dominant modes in Figure 5 are either very small, zero, or are slightly negative. This is evidence that the waves found downstream are not locally produced but rather convected from the area immediately adjacent to the shock. One can use homogeneous linear theory to provide additional arguments against local production of magnetosheath waves, as is demonstrated in Figure 6. The top panel of this figure shows the maximum growth rate for the AIC and mirror instabilities as a function of x, with

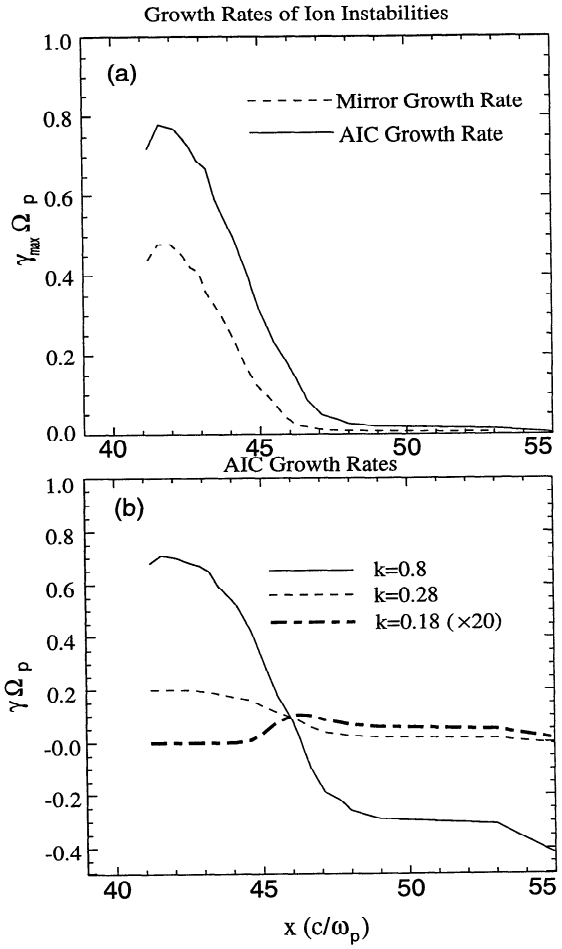

Figure 6. Linear growth rates calculated on the basis of local values of anisotropy and plasma beta of the simulation plasma at $\Omega_p t = 63$. (a) Maximum growth rates of the mirror instability (dashed line) and AIC instability (solid line). (b) Growth rates for the AIC instability for $k = 0.8c/\omega_{p1}$ (solid line), $k = 0.28c/\omega_{p1}$ (dashed line), and $k = 0.18c/\omega_{p1}$ (thick dashed line; γ multiplied by 10), where ω_{p1} is the downstream value of the plasma frequency.

the growth rate at each point based upon the values of the local ion anisotropy and plasma beta. As expected for a homogeneous electron-proton plasma, the AIC growth rate always exceeds the mirror. The growth rates for both instabilities peak at the shock ramp at values of the order of the ion gyrofrequency and decline rapidly thereafter. Within $12c/\omega_p$, $\gamma_{\max}$ of the AIC instability has dropped to threshhold levels, while the mirror mode is actually slightly damped. It must be stressed that this panel is only meant to provide a qualitative argument in support of the hypothesis that magnetosheath waves are produced near the shock. This is because homogeneous linear theory is not strictly applicable in the immediate vicinity of the shock, where steep gradients in plasma parameters are present and the ion distributions have complex structures (discussed below).

Note that for both instabilities the effective e-folding length projected along the shock normal is approximately independent of the group velocity and thus determined mostly by the growth rate. The mirror mode is a standing wave in the plasma rest frame and hence the only velocity associated with its propagation is the convection speed of the plasma. The strongest AIC modes propagate parallel to the magnetic field, which is nearly perpendicular to the shock normal. Hence convection by the plasma is generally far more important than propagation in determining the energy flux of Alfvén waves along the normal.

The bottom panel of Figure 6 shows the growth rate γ of the AIC instability as a function of x for three different wavenumbers ($\theta_{kB} = 0^o$ in each case). Assuming homogeneous linear theory is applicable near the shock front as well as further downstream, Figure 6b indicates that the AIC instability should be excited across a wide band of wavenumbers, with the fastest growing modes corresponding to relatively short wavelengths. However, within 10 ion inertial lengths of the shock the short-wavelength modes are heavily damped while longer-wavelength modes are either still growing or are only lightly damped. The longest wavelength modes actually experience more, albeit still only slight, growth at this point than they do right at the shock. Hence, from linear theory, one would expect long-wavelength modes to dominate the downstream and short-wavelength modes to dominate the near-shock region. For the AIC instability, the frequency of the dominant mode should also decrease as one moves away from the shock.

This is in fact true for the simulated shock and sheath. This can be seen in Figure 7, which shows the power at different values of k_y as functions of x for wave modes associated with (top panel) oscillations in the z direction and (bottom panel) compressional oscillations. At the shock, significant power is evident at values of $k_y c/\omega_p$ between 0.4 and 1.4 for trans-

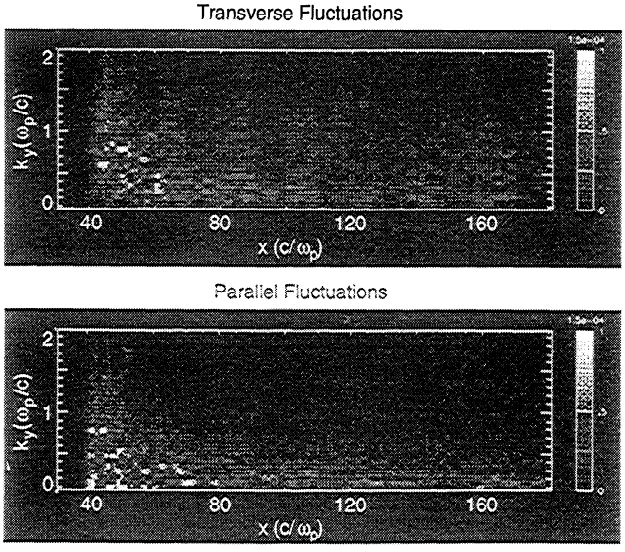

Figure 7. The power at different values of k_y as functions of x for wave modes associated with (top panel) oscillations in the z direction and (bottom panel) compressional oscillations at $\Omega_p t = 63$.

verse modes, and between 0.1 and 0.8 for compressional modes. Generally, for transverse oscillations, intensities at short wavelengths peak within a few c/ω_p of the shock and then decline rapidly in value. At intermediate wavelengths, intensities peak within about $10c/\omega_p$ of the shock and decline more slowly. The longest wavelength modes are often not visible at the shock but instead climb steadily in intensity, peak some tens of c/ω_p of the shock, and persist far downstream. For compressional oscillations, the picture is approximately the same except for the longest wavelength modes, which are intense near the shock as well as further downstream. Because of their dominance near the shock, where the ion anisotropy undergoes its fastest reduction, short-wavelength modes probably dominate the ion thermalization process. For AIC waves, these are also the higher frequency modes (ω/Ω_p between about 1.0 and 2.0 in upstream units and between 0.3 and 0.6 in downstream units). Further downstream, these higher frequency modes are damped out and AIC waves with frequencies ω/Ω_p below about 0.7 in upstream units and 0.2 in downstream units have the greatest intensities.

In summary, both the mirror mode and the Alfvén ion cyclotron mode have been identified in the simulated magnetosheath. They both are present at comparable intensities, with the intensities peaking near the shock front and then falling by an order of magnitude within several ion inertial lengths of the front. The amplitudes of these waves far downstream of the shock are too large to be explained by any local generation mechanisms. The fact that the mirror mode is competitive with the AIC mode also argues against local production. The simulation data support the idea that the wave activity observed far downstream is generated near the shock and convected away.

4. Ion Thermalization

In this section, we examine the evolution of the ion distribution function as the particles are energized in the shock ramp and then thermalized in the downstream plasma. For this study, we use the results from a second simulation that has upstream plasma parameters identical to the first, but for which the system dimensions have been reduced by a factor of 2 and the simulation is run for only $35\Omega_p^{-1}$. Figure 8 shows the profiles of the magnetic field magnitude and the temperature anisotropy averaged over y at $\Omega_p t = 35$. The peak values of both differ only slightly from those of the longer run, and the width of the shock ramp is about the same. The shaded areas indicate the sampling regions for the ion distribution functions shown in the next two figures. Each region is only one cell wide ($0.5c/\omega_p$) in x, but covers the whole range of y.

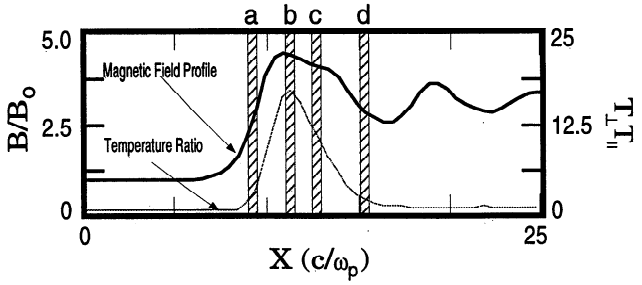

Figure 8. Profiles of B (black line) and $T_\perp/T_\parallel$ (gray line) for a simulation with the same parameters as the one with results shown in Figures 1-5, but with a smaller system size and shorter run time. Both quantities are averaged over y. The shaded areas indicate the sampling regions for the distribution functions shown in Figures 9 and 10. Region a corresponds to the top rows, region b to the second rows, region c to the third rows, and region d to the bottom row.

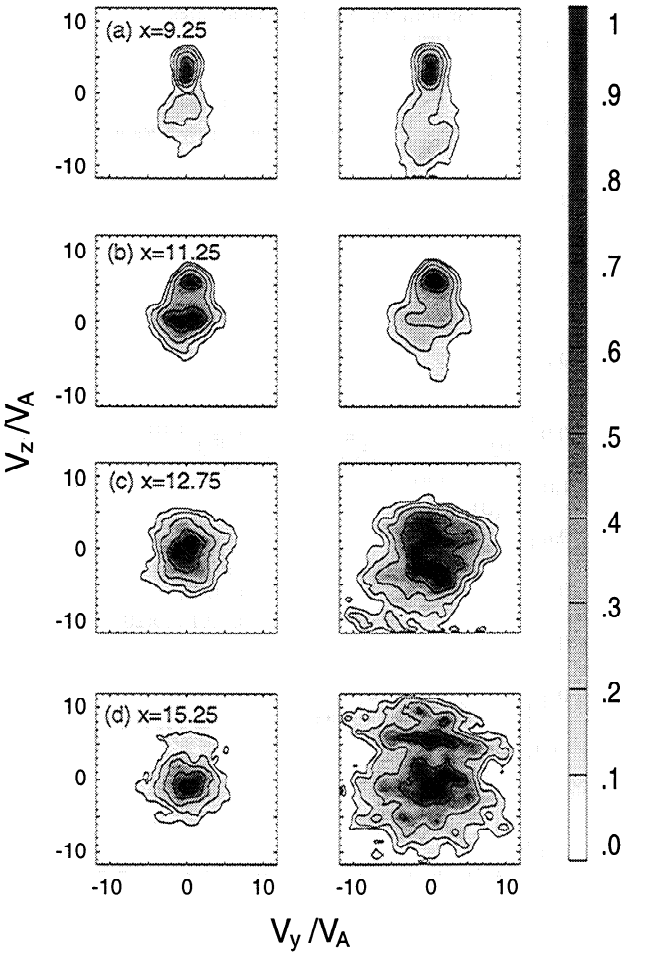

Figure 9. Contour and gray-scale plots of the ion distribution function (left side) and the energy distribution (right side) in $v_y - v_z$ space at four values of x. In each case, the distribution includes ions at all values of y and within $0.25c/\omega_p$ of the given value of x. Shown are the distributions at (top row) $x = 9.25c/\omega_p$, (second row) $x = 11.25c/\omega_p$, (third row) $x = 12.75c/\omega_p$, and (bottom row) $x = 15.25c/\omega_p$.

Figure 9 shows the evolution of the ion distribution function in v_z-v_y phase space, essentially plotting one component of $v_\perp$ (v_z) against $v_\parallel$ (v_y). The left column shows contours of the actual distribution function, while the right column shows the distribution of energy. Both distributions are measured in the downstream plasma rest frame. The values of x given here correspond to the

center of the cells. In each frame, the lowest contour level is 6.25% of the peak and each successive contour is twice the level of the previous one except the top contour, which is 75% of the peak level.

The top panels in Figure 9 show the ion distribution in the shock ramp. The incident distribution is stretched in the v_z direction as a result of the deflection of incident ions by the increased magnetic field in the ramp (see Figure 10). A reflected ion population with mostly negative v_z is also visible in both panels. This reflected population contains a disproportionate amount of energy even before the ions are fully transmitted. The second row of panels show the velocity and energy distribution at approximately the magnetic overshoot. At this stage the ion distribution consists of two distinct components: a core population of transmitted ions, centered approximately about the origin, and a smaller, halo population of initially reflected ions, centered about $(v_y, v_z) \simeq (0.0, 2.5)v_A$. As can be seen in the right panel, the halo population contains most of the energy in the system, about 60%, although it contains only about 20% of the total ion population. These fractions are consistent with observations of the proton halo at quasi-perpendicular shocks with $M_A \simeq 8$ [*Fuselier and Schmidt*, 1994]. The halo population also contains most of the free energy. In particular, its effective temperature anisotropy $A = T_\perp/T_\parallel$ is about 44, much larger than the core anisotropy of approximately 3.2.

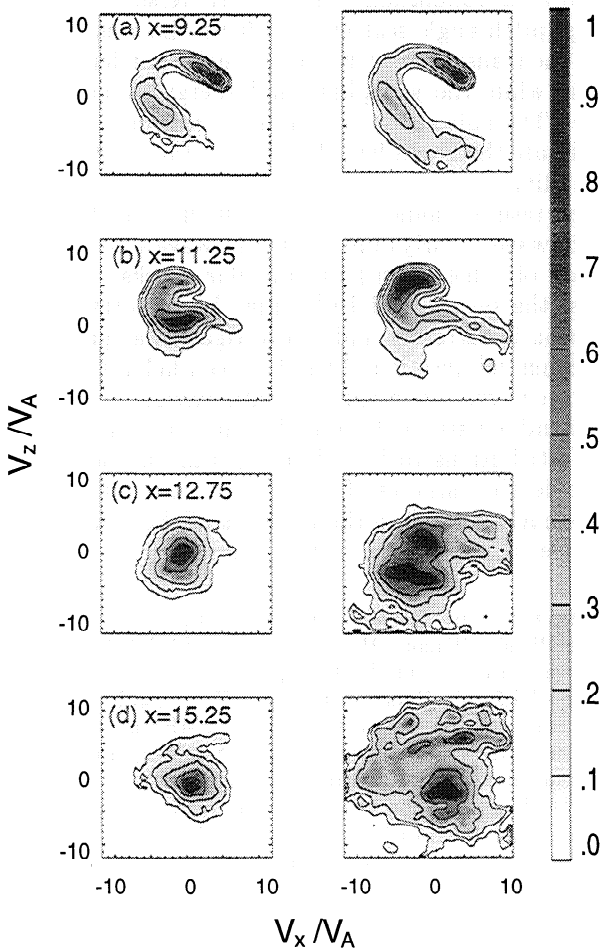

Figure 10. Contour and gray-scale plots of the ion distribution function (left side) and the energy distribution (right side) in $v_x - v_z$ space at four values of x. The format of this figure is the same as Figure 9.

The anisotropy of the total ion population drops by only about 13% (from A =15 to 13) between the second and third row of panels, but the structure of the distribution changes dramatically over this distance ($1.5c/\omega_p$). The ions in the halo component have diffused in v_z. The energy in the halo has also diffused across a much broader region of phase space, with energy diffusion strongest in v_z but also apparent in v_y. Within a few more ion inertial lengths (bottom row), the anisotropy has been reduced to about 3.1. Most of the remaining anisotropy is associated with the ions in the high-energy tail, which is easier to see in the energy distribution than in the velocity distribution. Particle energy has continued its spread across phase space, with much of the additional diffusion occurring in v_y as a result of the anisotropy reduction.

Figure 10 shows the same evolution, this time illustrating the particle and energy distributions in v_x-v_z phase space, essentially the perpendicular velocity phase space. The incoming beam and its specularly reflected counterpart are approximately centered about $(v_x, v_z) = (4.5, 2.0)v_A$ and $(-4.5, -2.0)v_A$, respectively. The top panels show the incident beam being deflected by the magnetic field in the ramp while most of the reflected ions are moving upstream. At the overshoot (second row), the halo and core components are as well defined in $v_x - v_z$ space as in $v_y - v_z$ space (Figure 9). The halo is strongly gyrophase-bunched, with most of the halo having phase angle ϕ (measured counterclockwise from the positive v_x axis) between 90° and 110°. A smaller part of the halo is located near $\phi = 0°$. By contrast, the core is more uniform. Again, the particle energy is concentrated in the halo and hence confined to a narrow range of gyrophase angle. Between the second and third rows, the halo ions diffuse along v_z with relatively little diffusion along v_x. Thus, at $x = 12.75c/\omega_p$, the ion distribution is still nongyrotropic but is relatively symmetric across the v_x axis. The core and halo populations both diffuse along the v_x and v_z axes between $x = 12.75c/\omega_p$ and $15.25c/\omega_p$ and hence are more gyrotropic in the bottom panels. The diffusion in ion energy in v_x-v_z phase space essentially reflects the particle diffusion.

Thus the shocked plasma evolves rapidly downstream of the shock. In the overshoot region, the free energy is concentrated in the reflected ion halo, which is highly anisotropic and gyrophase-bunched. Diffusion of the ions in gyrophase and energy begins before the anisotropy is reduced significantly by pitch-angle scattering. Within about $12c/\omega_p$, the distribution is approximately gyrotropic and nearly isotropic. This qualitative picture of ion evolution does not appear to be affected by the fact that the distributions displayed in Figures 8 and 9 are integrated over y. An examination of ion distributions in which the integration path along

y is $1/8L_y$ shows the same evolution as a function of x. Nor does it appear to be a function of simulation cell size. Examination of the ion distributions for a simulation in which cells are $0.25c/\omega_p$ wide in the x direction show approximately the same evolution. The picture derived from our simulations is similar to that provided by observations [*Paschmann et al.*, 1982; *Sckopke et al.*, 1983, 1990].

The energy/gyrophase diffusion and the anisotropy reduction occur as a result of the interaction of the halo population with the waves whose growth is fueled by the free energy in the initial shocked ion distribution. It is unclear at this stage how the interaction of these waves with the ions bring about energy diffusion and anisotropy reduction in the inhomogeneous environment near the shock. However, some clues can be derived by comparing the top panel of Figure 4 with the evolutionary sequence shown in Figures 9 and 10. Figure 4 indicates that the power in transverse oscillations peaks slightly downstream of the peak power in compressive oscillations and in fact the peak is located approximately in the region in which the ion anisotropy drops rapidly with x. Associating the transverse oscillations with AIC waves, one may conclude that these waves rather than mirror waves are responsible for the rapid anisotropy drop. This conclusion is supported by earlier works that have used homogeneous simulations to explore the issue of the competition between the mirror and AIC instabilities in the magnetosheath [*McKean et al.*, 1992, 1994]. The energy diffusion, on the other hand, may be due principally to compressive activity identified with mirror waves.

Further investigation of wave-particle interactions in the near-shock region is necessary before a comprehensive scenario of particle evolution in this region can emerge. Nonetheless, it is clear that the free energy in the nongyrotropic halo ions can generate compressive wave power at an equal level to transverse wave power, a feat that cannot be accomplished by a simple anisotropic bi-Maxwellian plasma, which preferentially excites the AIC mode.

5. Conclusion

Observations have identified mirror waves and Alfvén waves in the magnetosheath downstream of the quasi-perpendicular bow shock. Although kinetic theory has shown that in sheath-like, electron-proton plasmas the AIC mode should dominate the wave activity, the mirror mode often either dominates or is competitive with the AIC mode. The resolution of this conflict cannot be addressed adequately with one-dimensional simulations because typically only one wave mode can be modeled. Thus in this paper we have used two-dimensional hybrid simulations to model the quasi-perpendicular bow shock and the magnetosheath with the goal of resolving this conflict by following the evolution of the wave spectra and particle distribution functions downstream of the shock. Both the mirror mode and the Alfvén ion cyclotron mode have been identified in the simulated magnetosheath. They are both present at comparable intensities, with the intensities peaking near the shock front and then falling by an order of magnitude within several ion inertial lengths of the front. The far downstream waves cannot be explained by a local generation mechanism. The fact that the mirror mode is competitive with the AIC mode also argues against local production, for which linear theory would predict AIC dominance. Our simulation data support the idea that the wave activity observed far downstream is generated near the shock and convected away. Near the shock front, rapidly growing, short-wavelength modes dominate the wave spectrum. These modes are rapidly damped away, however, and further downstream long-wavelength modes dominate the wave activity.

The free energy that feeds the growth of these waves comes mostly from the halo of reflected ions that consists of only about 20% of the incident ion population but contains about 60% of the total ion energy. In the vicinity of the magnetic overshoot, the halo is concentrated in a narrow region of phase space and is both highly anisotropic and strongly gyrophase-bunched. The halo ions begin diffusing in gyrophase first, possibly through interacting with compressive waves, which are more prominent the first few ion inertial lengths behind the overshoot. Commensurate with this phase diffusion is a diffusion in ion energy away from the location of the initial halo population. As the transverse wave power grows, pitch-angle scattering reduces the anisotropy of both the transmitted core and the halo, particularly the latter, while the gyrophase and energy diffusion continue. The anisotropy is eventually reduced to the approximate threshold level for the excitation of the AIC instability.

Our results cannot explain observations that show mirror waves clearly dominating the wave activity downstream of some quasi-perpendicular shocks. For these cases, the presence of He^{++} may be important. This question is currently under investigation as part of the more general question of what impact helium ions have on the evolution of magnetosheath waves. We also plan to extend our study of the evolution of wave spectra and ion distributions to include low Mach number shocks. More detailed studies of the generation of waves in the near-shock region and the feedback of the waves on the particles are being planned as well.

Acknowledgments. This work was supported by NASA's Space Physics Theory Program, grant NAG 5-1492. Work performed by N. Omidi was supported under the auspices of the California Space Institute. Computations for this work were carried out on the CRAY YMP and C90 at the San Diego Supercomputing Center, which is operated by the National Science Foundation. We also thank P. Muret for his work in developing the diagnostic tools used here.

The Editor thanks S. A. Fuselier and another referee for their assistance in evaluating this paper.

References

Anderson, B. J., and S. A. Fuselier, Magnetic pulsations from 0.1 to 4.0 Hz and associated plasma properties in the Earth's subsolar magnetosheath and plasma depletion layer, *J. Geophys. Res.*, *98*, 1461, 1993.

Anderson, B. J., S. A. Fuselier, and D. Murr, Electromag-

netic ion cyclotron waves observed in the plasma depletion layer, *Geophys. Res. Lett., 18*, 1955, 1991.

Barnes, A., Collisionless damping of hydromagnetic waves, *Phys. Fluids, 9*, 1483, 1966.

Brinca, A. L., N. Sckopke, and G. Paschmann, Wave excitation downstream of the low-β, quasi-perpendicular bow shock, *J. Geophys. Res., 95*, 6331, 1990.

Byers, J. A., B. I. Cohen, W. C. Condit, and J. D. Hansen, Hybrid simulations of quasi-neutral phenomena in magnetized plasmas, *J. Comput. Phys., 27*, 363, 1978.

Chandrasekhar, S., A. N. Kaufman, and K. M. Watson, The stability of the pinch, *Proc. R. Soc. London A, 245*, 435, 1958.

Davidson, R. C., and J. M. Ogden, Electromagnetic ion cyclotron instability driven by ion energy anisotropy in high-beta plasmas, *Phys. Fluids, 18*, 1045, 1975.

Fuselier, S. A., and W. K. H. Schmidt, H^+ and He^{2+} heating at the Earth's bow shock, *J. Geophys. Res., 99*, 11,539, 1994.

Fuselier, S. A., D. M. Klumpar, E. G. Shelley, B. J. Anderson, and A. J. Coates, He^{2+} and H^+ dynamics in the subsolar magnetosheath and plasma depletion layer, *J. Geophys. Res., 96*, 21,095, 1991.

Gary, S. P., M. D. Montgomery, W. C. Feldman, and D. W. Forslund, Proton temperature anisotropy instabilities in the solar wind, *J. Geophys. Res., 81*, 1241, 1976.

Gary, S. P., The mirror and ion cyclotron anisotropy instabilities, *J. Geophys. Res., 97*, 8519, 1992.

Gary, S. P., S. A. Fuselier, and B.J. Anderson, Ion anisotropy instabilities in the magnetosheath, *J. Geophys. Res., 98*, 1481, 1993.

Gary, S. P., M. E. McKean, D. Winske, B. J. Anderson, R. E. Denton, and S. A. Fuselier, The proton cyclotron instability and the anisotropy/β inverse correlation, *J. Geophys. Res., 99*, 5903, 1994.

Hasegawa, A., *Plasma Instabilities and Nonlinear Effects*, Springer-Verlag, New York, 1975.

Hubert, D., C. Perche, C. C. Harvey, C. Lacombe, and C. T. Russell, Observation of mirror waves downstream of a quasi-perpendicular shock, *Geophys. Res. Lett., 16*, 159, 1989.

Kennel, C. F., and H. E. Petschek, Limit on stably trapped particle fluxes, *J. Geophys. Res., 71*, 1, 1966.

Lacombe, C. F., E. Kinzelin, C. C. Harvey, D. Hubert, A. Mangeney, J. Elaoufir, D. Burgess, and C. T. Russell, Nature of the turbulence observed by ISEE 1-2 during a quasi-perpendicular crossing of the Earth's bow shock, *Ann. Geophys., 8*, 489, 1990.

Lacombe, C. F., G. E. Pantellini, D. Hubert, C. C. Harvey, A. Mangeney, G. Belmont, and C. T. Russell, Mirror and Alfvénic waves observed by ISEE 1-2 during crossings of the Earth's bow shock, *Ann. Geophys., 10*, 772, 1992.

Lee, L. C., C. P. Price, C. S. Wu, and M. E. Mandt, A study of mirror waves generated downstream of a quasi-perpendicular shock, *J. Geophys. Res., 93*, 247, 1988.

McKean, M. E., D. Winske, and S. P. Gary, Mirror and ion cyclotron anisotropy instabilities in the magnetosheath, *J. Geophys. Res., 97*, 19,421, 1992.

McKean, M. E., D. Winske, and S. P. Gary, Two-dimensional simulations of ion anisotropy instabilities in the magnetosheath, *J. Geophys. Res., 99*, 11,141, 1994.

Moustaizis, S., D. Hubert, A. Mangeney, C. C. Harvey, C. Perche, and C. T. Russell, Magnetohydrodynamic turbulence in the Earth's magnetosheath, *Ann. Geophys., 4A*, 355, 1986.

Omidi, N., A. O'Farrell, and D. Krauss-Varban, Sources of magnetosheath waves and turbulences, *Adv. Space Res., 14*(7), 45, 1994.

Paschmann, G., N. Sckopke, S. J. Bame, and J. T. Gosling, Observations of gyrating ions in the foot of the nearly perpendicular bow shock, *Geophys. Res. Lett., 9*, 881, 1982.

Price, C. P., D. W. Swift, and L. C. Lee, Numerical simulation of nonoscillatory mirror waves at the Earth's magnetosheath, *J. Geophys. Res., 91*, 101, 1986.

Sckopke, N., G. Paschmann, J. T. Gosling, and C. T. Russell, Evolution of ion distributions across the nearly perpendicular bow shock: Specularly and nonspecularly reflected gyrating ions, *J. Geophys. Res., 88*, 3046, 1983.

Sckopke, N., G. Paschmann, A. L. Brinca, C. W. Carlson, and H. Luhr, Ion thermalization in quasi-perpendicular shocks involving reflected ions, *J. Geophys. Res., 95*, 6337, 1990.

Tsurutani, B. T., E. J. Smith, R.R. Anderson, K. W. Ogilvie, J. D. Scudder, D. N. Baker, and S. J. Bame, Lion roars and nonoscillatory drift mirror waves in the magnetosheath, *J. Geophys. Res., 87*, 6060, 1982.

Winske, D., and K. B. Quest, Magnetic field and density fluctuations at perpendicular supercritical collisionless shocks, *J. Geophys. Res., 93*, 9681, 1988.

Yoon, P. H., Quasi-linear evolution of Alfvén/ion-cyclotron and mirror instabilities driven by ion temperature anisotropy, *Phys. Fluids, B4*, 3627, 1992.

Zwan, B. J., and R. A. Wolf, Depletion of solar wind plasma near a planetary boundary, *J. Geophys. Res., 81*, 1636, 1976.

D. Krauss-Varban, M. E. McKean, and N. Omidi, Department of Electrical and Computer Engineering, University of California, San Diego, La Jolla, CA 92093-0407.
(e-mail: mmckean@ece.ucsd.edu; mem@demos.lanl.gov)

(Received May 31, 1994; revised August 30, 1994;
accepted September 22, 1994.)